Revista GEOCIÊNCIAS

unesp

ISSN: 1980-900X (online)

Chl-a ESTIMATION FROM RS TECHNIQUES: COMPARATIVE ANALYSIS OF DATA ACQUIRED BY SATELLITES AND RPA

TÉCNICAS DE SENSORIAMENTO REMOTO PARA ESTIMATIVA DE Chl-a: ANÁLISE COMPARATIVA DE DADOS ADQUIRIDOS POR SATÉLITES E RPA

Cinthya de Souza Marinho[1], Tati De Almeida[2], Guilherme Gomes Pessoa[1], Henrique Llacer Roig[2], Lucas da Silva Dias[2], Miguel Oliveira da Costa[1], Rejane Ennes Cicerelli[2],

[1]Geoscience Institute, University of Brasília, Câmpus Universitário Darcy Ribeiro, Brasília, DF – Brazil.
E-mails: cinthya@aluno.unb.br; guilherme.pessoa@unb.br; miguel-oliveira.mo@aluno.unb.br;

[2]Applied Geosciences and Geodynamics, Geoscience Institute, University of Brasília, Câmpus Universitário Darcy Ribeiro, Brasília, DF - Brazil.
E-mails: tati_almeida@unb.br; roig@unb.br; lucas.dias@aluno.unb.br; rejaneig@unb.br

RESUMO - A composição e a concentração da biomassa de algas são indicadores-chave da qualidade da água e dos níveis de eutrofização em ambientes lênticos e lóticos. A estimativa das concentrações de algas tem sido um foco central da pesquisa em sensoriamento remoto, com avanços recentes em modelagem e aquisição de dados visando reduzir erros associados a sistemas de aquisição e à variabilidade ambiental. Este estudo desenvolveu uma estratégia para monitorar a clorofila-a usando imagens multiespectrais de alta resolução espacial em uma região impactada por fontes de poluição pontuais e difusas, especificamente na foz do Riacho Fundo no Lago Paranoá, Distrito Federal, Brasil. Os dados foram adquiridos por meio de imagens de satélite PlanetScope e de um sistema de Aeronave Remotamente Pilotada (APR), juntamente com medições limnológicas, meteorológicas e de Reflectância de Sensoriamento Remoto (Rrs) *in situ*. Modelos de regressão linear estatisticamente validados mostraram fortes correlações entre dados de sensoriamento remoto e concentrações de clorofila-a, com valores de R^2 de 0,80 para dados de APR (canal vermelho: 640–680 nm) e 0,81 e 0,72 para dados do PlanetScope (verde: 500–590 nm; vermelho: 590–670 nm). Essas descobertas destacam o potencial dos sistemas de sensoriamento remoto por satélite e APR para estimar a clorofila-a em águas continentais, mesmo em condições de baixa biomassa. No entanto, a precisão do modelo pode ser reduzida em águas muito claras, sob mudanças sazonais nas propriedades ópticas ou sem calibração regular do sensor.
Palavras-chave: Clorofila-*a*.·Sensoriamento remoto. Qualidade da água. PlanetScope. APR.

ABSTRACT - The composition and concentration of algal biomass are key indicators of water quality and eutrophication levels in both lentic and lotic environments. Estimating algal concentrations has been a central focus of remote sensing research, with recent advances in modeling and data acquisition aimed at reducing errors associated with acquisition systems and environmental variability. This study developed a strategy for monitoring chlorophyll-a using high-spatial-resolution multispectral imagery in a region impacted by both point and diffuse pollution sources, specifically at the mouth of Riacho Fundo in Paranoá Lake, Federal District, Brazil. Data were acquired from PlanetScope satellite imagery and a Remotely Piloted Aircraft (RPA) system, alongside limnological, meteorological, and in situ Remote Sensing Reflectance (Rrs) measurements. Statistically validated linear regression models showed strong correlations between remote sensing data and chlorophyll-a concentrations, with R^2 values of 0.80 for RPA data (red channel: 640–680 nm) and 0.81 and 0.72 for PlanetScope data (green: 500–590 nm; red: 590–670 nm). These findings highlight the potential of RPA and satellite remote sensing systems for estimating chlorophyll-a in continental waters, even under low-biomass conditions. However, model accuracy may be reduced in very clear waters, under seasonal shifts in optical properties, or without regular sensor calibration.
Keywords: Chlorophyll-*a*. Remote Sensing. Water quality. PlanetScope. UAV.

INTRODUÇÃO

Eutrophication is a major consequence of pollution in aquatic environments, driven by nutrient enrichment that stimulates excessive phytoplankton growth and can lead to harmful algal blooms (HABs). Such blooms deteriorate water quality, deplete dissolved oxygen, disrupt ecological balance, and may release toxins that threaten aquatic life and limit water usability (Walker, 2025; Lan et al., 2025).

Phytoplankton biomass is widely recognized

as a robust proxy for eutrophication levels, as excessive phytoplankton growth directly indicates nutrient enrichment in aquatic environments. Chlorophyll-a (Chl-a), a primary photosynthetic pigment, is widely used to estimate phytoplankton concentration and, consequently, to assess the trophic status of water bodies (Khan et al., 2021). Remote sensing (RS) techniques have become increasingly important tools for Chl-a estimation, providing synoptic, non-invasive monitoring. However, the performance of RS-based estimations is strongly influenced by sensor characteristics, including spatial, spectral, and radiometric resolution (Kumar et al., 2025; Izadi et al., 2021; Rolim et al., 2023; Lobo et al., 2021; Maciel et al., 2020, 2023). Satellite-based RS has been extensively used for water quality monitoring (Tesfaye, 2024; Lobo et al., 2021; Maciel et al., 2020, 2023).

Sensors such as PlanetScope provide high spatial and temporal resolution but are often limited by lower radiometric quality and susceptibility to cloud cover (Mansaray et al., 2021). Along with Chl-a, other photosynthetic pigments – such as phycocyanin, phycoerythrin, carotenoids, and xanthophylls – can also be monitored via remote sensing, albeit with certain limitations. For instance, Markogianni et al. (2020) monitored Chl-a in lakes in Greece from medium-resolution imagery, with an RMSE of 1.3 mg/m³. Similarly, Maciel et al. (2020) reported a coefficient of determination (R^2) of 0.56 for remote sensing reflectance in the PlanetScope sensor bands in turbid waters but obtained poor results in clear lakes ($R^2 = 0.08$). These limitations are particularly critical in small or complex inland waters, where mixed pixels and variable optical conditions affect accuracy (Maciel et al., 2020; Markogianni et al., 2020).

In contrast, Remotely Piloted Aircraft (RPA) platforms have emerged as a powerful alternative for water quality monitoring. RPAs can operate below cloud cover, providing centimeter-level spatial resolution and enabling flexible, on-demand data acquisition (Ngwenya et al., 2025; Olivetti et al., 2020, 2023). Recent studies demonstrate the feasibility of using RPAs equipped with multispectral or hyperspectral sensors to accurately estimate Chl-a concentrations and detect phytoplankton blooms (Olivetti et al., 2023). Shang et al. (2017) demonstrated the use of a hyperspectral sensor coupled with a low-cost, low-altitude RPA to monitor phytoplankton blooms (Phaeocystis globosa), revealing Chl-a concentrations between 7.3 and 45.6 mg/m³. This capability enhances the spatial and temporal resolution of monitoring programs, complementing satellite observations and reducing reliance on sparse in situ sampling.

Given this context, it is crucial to evaluate the performance, advantages, and limitations of Chl-a estimation from both satellite and RPA data. This study focuses on a comparative analysis of these two RS platforms applied to a critical area of Paranoá Lake (Brasília, DF), specifically the Riacho Fundo arm, which is strongly influenced by anthropogenic activities and multiple pollution sources (De Aquino et al., 2018; Dias and Baptista, 2015). By analyzing and comparing the accuracy and applicability of satellite- and RPA-derived data for Chl-a estimation, this research aims to support the development of more effective strategies for monitoring water quality in inland aquatic ecosystems.

MATERIALS AND METHODS

The study area is located within Paranoá Lake, a large, man-made reservoir in the Federal District of Brazil, covering a total area of 4,800 hectares. The lake plays a crucial role in supplying water to surrounding urban areas, but it also faces significant environmental challenges due to urbanization and pollution. The study area comprises 38 hectares located in the Riacho Fundo arm of Paranoá Lake. Its selection considered not only operational aspects, such as the flight autonomy of the Remotely Piloted Aircraft (RPA) employed, but also its scientific relevance. Long-term monitoring conducted by the Environmental Sanitation Company of the Federal District (CAESB) over an 11-year period (2006–2017) has consistently identified this arm as the most impacted sector of the reservoir. Average chlorophyll-a (Chl-a) concentrations of 13.12 mg/m³ classify the site as eutrophic according to Carlson's Trophic State Index, as modified by Lamparelli (2004), with values ranging from 0 to 98.4 mg/m³. The combination of multiple pollution sources, high temporal variability, and documented eutrophication makes this area a representative natural laboratory for testing and validating remote sensing approaches to water quality monitoring.

Characterized by a "Tropical Savanna" climate according to Köppen's classification, the area has

a well-defined rainfall regime, with the rainy season occurring from October to April (Codeplan, 1984), during which 84% of the total annual rainfall (ranging from 1200 to 1700 mm) is concentrated. This same area was the focus of studies by Batista and Fonseca (2018), who investigated phytoplankton, and by Mar da Costa et al. (2016), who examined biogeochemical mechanisms for controlling trophic state and micropollutant concentrations.

This environment is impacted by both diffuse and point-source pollution from various sources, including effluents from the Sewage Treatment Plant (ETE Sul) (Dias and Baptista, 2015), discharges from the Riacho Fundo stream (De Aquino et al., 2018), stormwater and surface runoff (Fonseca, 2001), potential illegal sewage connections, and improper solid waste disposal. The diversity and complexity of these pollution sources have led to fluctuating pollutant concentrations over time, highlighting the need for high-resolution, spatially detailed monitoring. This area is subjected to significant anthropogenic pressures, including urban runoff, treated and untreated wastewater discharges, diffuse pollution from densely populated areas, and agricultural runoff (De Aquino et al., 2018; Dias and Baptista, 2015).

Figure 1 shows the data collection locations, numbered 1 to 10, which were defined using the accumulated reflectance technique (Almeida et al., 2018).

This method is effective for identifying regions of spectral variability and is particularly useful for classifying and identifying vegetation types and water composition in areas with climatic seasonality (Hermuche and Sano, 2011; Grande et al., 2016). To apply the technique, the sum of eight PlanetScope Surface Reflectance images collected over a two-year period was used.

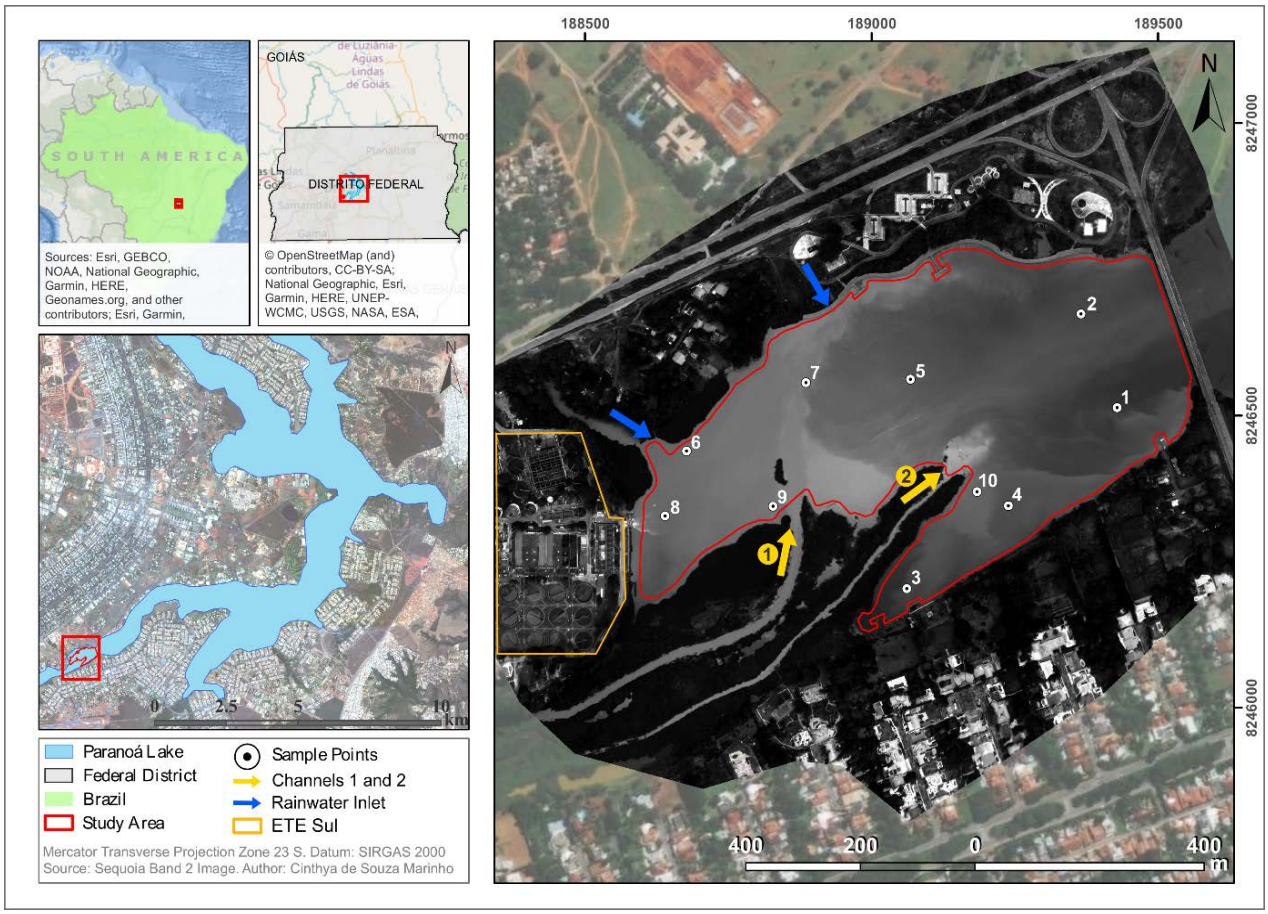

Figure 1 - Study area and sampling points distribution

DATA ACQUISITION

In its various stages, this study explores data from three sources: field data, orbital data, and RPA airborne data. Field data include in situ limnological, meteorological, and remote sensing reflectance (Rrs) variables. Orbital data refers to PlanetScope (PS) imagery. RPA airborne data consists of images acquired using the Sequoia multispectral sensor. Whenever possible, the simultaneous acquisition of all data types was prioritized. To this end, the acquisition of orbital,

airborne, and field data was planned for the same dates.

Initially, four field campaigns were planned throughout 2019, all of which were carried out as scheduled. The data collection took place on the following dates: May 6, 2019 (N=3), July 1, 2019 (N=10), October 11, 2019 (N=3), and December 6, 2019 (N=10). During these campaigns, limnological, meteorological, and field spectrometry data were collected. In order to increase the density of field data, additional campaigns were conducted focusing solely on chlorophyll-a data collection. These data were obtained on September 23, 2019 (N=6). Additionally, six other campaigns were carried out by CAESB at different times that year, with N=1 for each field survey: January 23, 2019; May 27, 2019; June 19, 2019; July 23, 2019; September 17, 2019; and February 11, 2020.

PS images were acquired for all field campaigns, but exact date matching was not always possible, leading to gaps of 1 to 3 days. Additionally, no PS images were available for the May 6, 2019 campaign due to excessive cloud cover. RPA images were acquired only for the campaigns on July 1, 2019, and December 6, 2019. These images were captured at different flight altitudes, resulting in varying ground sample distances (GSD). Table 1 presents a summary of the acquired data, including the field campaign date, image acquisition date, cloud cover percentage, number of limnological data collection points, flight altitude, and pixel size.

Aerial images were acquired using a Parrot Sequoia multispectral sensor mounted on a DJI Phantom 4 RPA. The Sequoia sensor is equipped with four 1.2-megapixel monochrome cameras that operate in narrow spectral bands: green (530–570 nm), red (640–680 nm), red-edge (730–740 nm), and near-infrared (770–810 nm), with bandwidths of 40 nm for the green, red, and NIR bands, and 10 nm for the red-edge band. In addition, the system includes an integrated RGB camera, a built-in GNSS receiver, and a solar irradiance sensor with spectral filters corresponding to each multispectral band (Parrot, 2017). The solar sensor measures incident irradiance at the moment of image capture, which supports the radiometric correction process. To ensure accurate conversion of the raw images to surface reflectance during orthomosaic generation, a calibrated reflectance panel was used during flight operations.

Images were acquired at nadir with a low solar angle to minimize Sun Glint, a phenomenon caused by the reflection of direct solar radiation when light strikes a surface and is reflected at the same angle of incidence (Ortega-Terol et al., 2017). To reduce this effect, flights were conducted in the morning, between 8 AM and 9 AM. To ensure accurate positioning of photo-identifiable natural targets and improve the geometric correction of Sequoia-generated products, a geodetic survey was conducted using high-precision Trimble R8s RTK GNSS receivers.

Analytic SR products from the "PlanetScope Ortho Scene Product" category were used to provide surface reflectance (%) data. These orthorectified products offer a nominal spatial resolution of approximately 3.7 m at nadir and an orthorectified pixel size of 3.0 m. They feature a 12-bit radiometric resolution, scaled and delivered in 16-bit, and include four spectral bands: Blue (B) (455–515 nm), Green (G) (500–590 nm), Red (R) (590–670 nm), and Near-Infrared (NIR) (780–860 nm). The spectral bandwidths are 60 nm for B, 90 nm for G, and 80 nm for R and NIR (Planet, 2020).

In situ Rrs hyperspectral data were acquired by the RAMSES TriOS spectroradiometer. This data can be considered as ground truth for the evaluation of airborne and orbital products. To measure the in situ Rrs of the apparent optical property (AOP) at the collection points, the structure and geometry proposed by Villar et al. (2013) and Martinez et al. (2015) were used. In situ Rrs values were obtained using Eq. 1 (Mobley, 1999).

$$R_{rs} = (Lu - Ld*p)/Ed \quad (1)$$

Where: Lu = upwelling radiance of the water surface; Ld = radiance of the atmosphere; Ed = downwelling irradiance; P = proportional factor, in this case, 0.028 was used, a low-variability value according to conditions and settings defined by Mobley (1999) and applied in this work.

The in situ Rrs data were resampled according to the Relative Spectral Response (RSR) of the PlanetScope sensor bands, according to Eq. 2, which uses the image band gain for the calculation (Rotta et al., 2016).

$$R_{rs\_r}(\lambda) = \frac{\Sigma_\lambda (R_{sr}(\lambda) * S(\lambda))}{\Sigma_\lambda S(\lambda)} \quad (2)$$

Where: Rrs_r (λ) = resampled Rrs value for each band of the respective sensors; S (λ) = value of the band gain function, or relative spectral

response to the wavelengths for each band interval of the respective sensors.

The in situ Rrs data were compared with data from the Sequoia and PlanetScope sensors to assess their radiometric quality. For this purpose, regression analysis was performed between the in situ Rrs data resampled for the spectral range of each sensor and the corresponding Rrs data from the sensors.

Chl-a concentrations were determined through water collection and laboratory analysis, following the "Spectrophotometric determination of chlorophyll" method described in APHA, AWWA, and WEF (2017), the same protocol used by CAESB.

Water samples were collected in duplicate using one-liter dark bottles, stored in a cooler with ice, and maintained under appropriate temperature and light conditions throughout the laboratory process. Filtration was performed using Whatman GF/F (0.7 µm) glass fiber filters. Additionally, other limnological variables were measured using an EXO 2 multiparameter probe (Table 2).

Based on field chlorophyll-a data and calibrated radiometric data from both sensors, models commonly used in the literature to estimate Chl-a were tested for Sequoia and PlanetScope data. For the Sequoia models, the 10 sampling points from the December campaign were used. For the PlanetScope models, a total of 23 points were utilized, drawn from the July 1, 2019, September 23, 2019, and October 11, 2019 campaigns, as well as the six CAESB campaigns.

Pixel extraction maintained approximately the same area around the sampling points for the different campaigns. For the July field campaign, due to lower flight height and smaller pixel size (Table 1), the extraction was done in 8×8 pixels, totaling 1.08 m² per sampling point. For December, the extraction was 3×3 pixels, totaling 1.06 m² per sampling point. The average pixel value was used for data analysis. The construction of the orthomosaics was performed using Pix4Dmapper software. The extraction of pixels from the PS images was performed in a 3×3 window around each sampling point, and the average for each point was calculated.

Table 1 - PlanetScope scenes used in the research and configuration of the Sequoia and RPA system

	PlanetScope					
Field Date	Acquisition Date	Satellite ID	Sight angle (nadir)	NV* %	Number of Points	Observations
01/July/2019	02/July/2019	1044	5°	0,0	10	01 day gap between field and image
23/Sep/2019	24/Sep/2019	0f44	4.9°	0,0	6	01 day gap between field and image
11/Oct/2019	14/Oct/2019	1029	0.2°	1,0	3	03 days gap between field and image
06/Dec/2019	-	-	-	-	10	Images near field with high % NV
23/01/19 – Caesb	23/Jan/2019	103a	2°	5,0	1	CAESB field
27/05/19 - Caesb	27/May/2019	0e2f	5°	0,0	1	CAESB field
19/06/19 - Caesb	19/Jun/2019	1057	3°	1,0	1	CAESB field
23/07/19 - Caesb	23/Jul/2019	1058	4.1°	5,0	1	CAESB field
17/09/19 - Caesb	17/Sep/2019	1048	4°	0,0	1	CAESB field
11/02/.20 - Caesb	11/Feb/2020	0e19	6.3°	8,0	1	CAESB field

	Sequoia				
Field Date	Overlap	Flight speed	Flight height	Pixel size	Coverage area
01/July/19	Frontal: 80% Lateral: 65%	12 m/s	120 m	13.02 cm	1.029 km^2
06/Dec/19			310 m	34.34 cm	1.642 km2

*NV = Cloud

To evaluate the statistical significance of the correlation coefficient between chlorophyll-a concentrations and surface reflectance pixel values from Sequoia and PlanetScope images, the Student's t distribution was applied to the best Chl-a estimation models for each sensor. The test statistic was calculated using Eq. 3 (Bussab and Morettin, 1987).

$$t = r\sqrt{\frac{n-2}{1-r^2}} \quad (3)$$

Where: t = Student's t distribution, with n−2 degrees of freedom; r = correlation coefficient.

Additionally, the multiple sub-sample method

known as jackknife (Lachenbruch, 1967) was used to validate the Sequoia regression model. This technique is particularly useful for studies with limited sample data, making it well-suited for the Sequoia model, which was based on only 10 sample points.

Furthermore, confidence intervals (Morettin and Bussab, 2002) were calculated using BioEstat software, version 5.0, along with the Root Mean Square Error (RMSE), as given in Eq. 4 (Darvishzadeh et al., 2008).

For the PlanetScope models, validation was performed by randomly removing three of the 23 sampling points from the initial model to calculate RMSE and confidence intervals.

A new regression analysis was then conducted using the remaining 20 sampling points, correlating PS Rrs data with Chl-a concentrations to establish the final estimation model for this parameter.

$$\mathrm{RMSE} = \left\{\frac{1}{2}\sum_{i=1}^{n}[(q_i \text{ estimado}) - (q_i \text{ medido})]^2\right\}^{\frac{1}{2}} \quad (4)$$

Where q = parameter of interest, n = number of samples.

After completing the statistical analyses, the best regression models for PlanetScope and Sequoia were applied to spatially represent the distribution of Chl-a in the reservoir. The results were then compared to propose an effective method for Chl-a monitoring.

RESULTS AND DISCUSSION

Water Quality Analysis

Laboratory tests on water samples collected during the field campaigns revealed that, in all cases, average Chl-a concentrations remained below 10 mg/m³, the threshold established by the National Environment Council (CONAMA, Brazil, 2005) for Class I waters.

This limit also aligns with the World Health Organization (WHO) standard for relatively low probabilities of adverse health effects (Binding et al., 2020). According to Lamparelli's (2004) classification, the water body was categorized as oligotrophic in May and July, while in September, October, and December, it shifted to a mesotrophic state. An exploratory analysis of water quality and meteorological data is presented in Table 2.

Data presented in Table 2 were obtained from different sources: weather data refers to precipitation acquired from automatic and conventional stations (located at Lat -15.79º, Long -47.93º, Altitude 1160.96 m) available at https://tempo.inmet.gov.br/; Cond. was collected by the Exo probe; and monthly precipitation was estimated by accumulating precipitation from 30 days before collection.

Table 2 Average values of physical, chemical and biological limnological variables collected, and weather data from field surveys in the mouth of Riacho Fundo

Field dates and N	Physical/chemical and biological limnological data						Weather data					
	Chl-a mg/m³	Cond.	O2 dissolv. mg/L	TDS mg/L	Turb. (NTU)	pH	Temp. min-max (°C)	Wind speed (m/s)	Wind direc-tion	Um (%)	Daily Precipi-tation. (mm)	Monthly Precipita-tion (mm)
	ref: 30		ref: > 5 mg/L	ref.: 500	ref: 100	ref: 6.0 a 9.0						
06/05/19	1.43	...	...	...	...	...	18.5-27.5	2	2.06°	71	0.0	372.6
01/07/19	2.06	200.9	5.79	136.98	10.98	7.29	12.6-26.3	0	0°	51	0.0	8.0
23/09/19	5.03	145.9	8.73	100.78	10.37	8.09	20.3-30.2	6.2	14°	38	0.0	0.0
11/10/19	5.93	...	...	...	...	...	17.7-29.2	5.14	14°	56	0.6	15
06/12/19	3.86	234.2	5.27	158.66	30.45	7.37	19.4-29	0	0°	83	72.4	310.8

N: number of sample elements; *Cond.*: conductivity (µS/cm); *Turb.*: turbidity; *TDS*: Total Dissolved Solids; Um.: average relative humidity. *ref:* reference values according to CONAMA Resolution number 357/2005 for class II of fresh water. *'...':* unknown data, as no probe collections were performed in these fields.

In general, the Chl-a concentrations obtained in this study are considered low for remote sensing detection. Most studies monitoring this variable in water typically report higher concentrations. For instance, Cicerelli and Galo (2015) observed an average concentration of 47.54 mg/m³, while Shang et al. (2017) recorded values ranging from 6 to 98 mg/m³. Similarly, Pahlevan et al. (2020) reported concentrations between 3.9 and 41.9 mg/m³, and Cheng et al. (2020) found

values between 0.12 and 38.57 mg/m³. Successful quantitative mapping of Chl-a in coastal waters using RPA has generally been achieved at concentrations above 15–20 mg/m³. Zhao et al. (2023) developed a regression method to estimate Chl-a concentration using multispectral data collected by UAVs, with concentrations ranging from approximately 10 to 20 mg/m³.

During December's rainy season—with a monthly rainfall of 310.8 mm (Table 2) — both turbidity and Total Dissolved Solids (TDS) increased, although they remained below CONAMA's Class II limit of 100 NTU. Dissolved oxygen and pH levels were also within the acceptable range for Class II waters. Furthermore, the strong correlations observed between turbidity and TDS ($R^2 = 0.95$ in July and $R^2 = 0.92$ in December) indicate that suspended solids are the primary contributors to turbidity.

Precipitation volumes recorded during the field surveys were consistent with the typical range for the Riacho Fundo sub-basin. However, April's rainfall was notably atypical, reaching approximately 320 mm compared to the usual 133 mm (INMET, 2020).

Spectral response and spectral analysis of sequoia and Planetscope Imagery

Comparing the spectral reflectance curves from December and July (Figure 2) reveals a broader range and higher reflectance intensity in December, reaching up to approximately 3.5% due to increased turbidity from rainfall, which enhances the reflectance signal, compared to a maximum of 1.5% in July.

Despite these differences, both datasets clearly exhibit the characteristic spectral signatures of chlorophyll-a, including green reflectance around 550 nm, red absorption near 665 nm, and red-edge reflectance between 690 and 705 nm (Astuti et al., 2018). These features, although subtle due to the overall low chlorophyll-a concentrations (averaging 2.95 mg/m³, Table 2), confirm the presence of chlorophyll in both periods. The observed spectral behavior aligns with the findings of Maciel et al. (2019), who reported similar patterns at higher minimum chlorophyll-a concentrations (averages of 21.97 mg/m³ and 31.11 mg/m³).

Group 1 (Figure 2), highlighted in a darker color, comprises three sample points (6, 8, and 9) that display TSS characteristics—namely, high reflectance in the green and red regions (550–700 nm) with a decline toward the near-infrared (NIR) (Giardino et al., 2017).

These points are closely clustered and located near the channel with the highest flow entering the mouth of Riacho Fundo (Figure 1), suggesting that increased suspended solids from the inflowing water are responsible for this spectral behavior. In contrast, Group 2, which includes the remaining sample points, exhibits the typical spectral features of chlorophyll-a, such as a maximum reflectance in the green region, confirming the presence of this pigment in the water.

Figure 3 compares the Rrs spectra from the Sequoia and PlanetScope sensors with field spectral reflectance measurements. The dashed lines represent the average sensor data, while the dark solid lines show the resampled in situ Rrs spectra for each sensor. Both sensors display elevated reflectance intensities and exhibit absorption and reflection patterns similar to those observed in field spectroradiometry. In particular, Sequoia's spectral data closely align with the *in situ* measurements, notably showing increased reflectance intensity in December after rainfall.

Comparing the spectral responses between July and December, distinct patterns emerge. In July, Sequoia exhibited its highest reflectance in the green band (centered at 550 nm) and lower reflectance in the red band (centered at 660 nm), a characteristic signature of chlorophyll-a. In contrast, December showed a shift in spectral behavior, with the highest reflectance occurring in the red band, similar mean reflectance values in both the green and red bands, and a decline toward the NIR band. The absence of a red-edge band around 705 nm in Sequoia limits a more precise assessment of chlorophyll-a, but the observed spectral differences between the two months suggest variations in water composition, likely influenced by seasonal changes and rainfall events.

Regression analyses were performed between the *in situ* Rrs and the Rrs values obtained from each sensor, revealing different correlation patterns across spectral bands and months. In the December campaign, Sequoia's Rrs showed strong correlations with in situ Rrs, with coefficients of determination (R^2) of 0.00, 0.64, 0.84, and 0.89 for the green, red, red-edge, and NIR bands, respectively. Due to these significant relationships, only December data were used to develop the Sequoia Chl-a predictive model. In

contrast, the July dataset lacked correlations between in situ Rrs, Sequoia Rrs, and Chl-a concentrations, making it unsuitable for predictive modeling. Similarly, the PlanetScope sensor did not show any correlation with *in situ* Rrs or Chl-a concentrations in July.

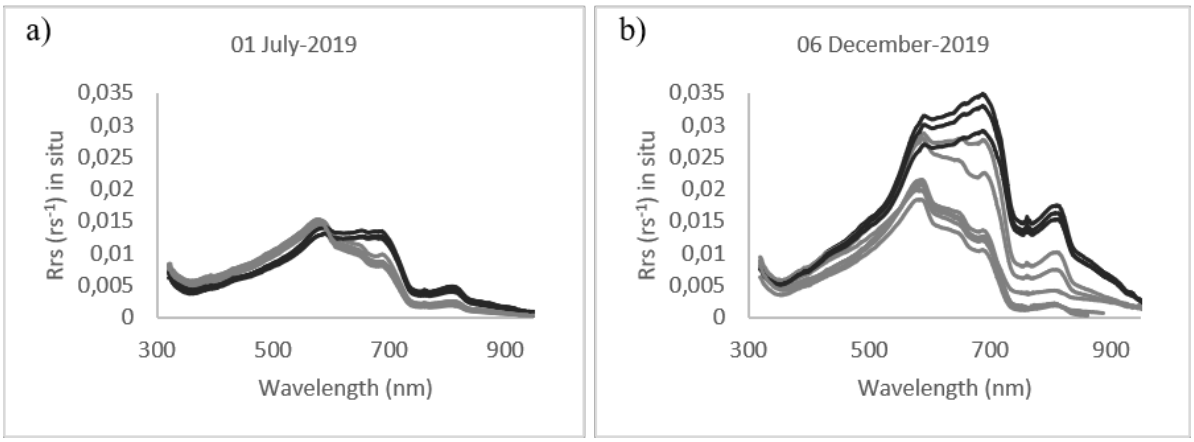

Figure 2 - Field Remote Sensing Reflectance (Rrs) spectra from the July a) and December b) campaigns.

These results are likely influenced by the low reflectance intensity observed in July (Figure 2 and Figure 3) and the low concentrations of optically active components (OACs) recorded during that campaign (Table 2).

Several studies have reported similar interferences. For instance, Maciel et al. (2020) found that in clear water, a low TSS concentration (3.66 mg/L) significantly increased errors in PS image analyses compared to turbid water conditions (TSS = 25.87 mg/L). Likewise, Pahlevan et al. (2014) demonstrated that the OLI sensor is capable of detecting Chl-a variations above 0.5 mg/m³; however, this sensor benefits from a relatively higher signal-to-noise ratio (SNR). The lower the backscatter, the lower the Rrs values, and such low Rrs levels demand a higher SNR than what PS sensors provide (Traganos et al., 2017) to minimize noise in the final results.

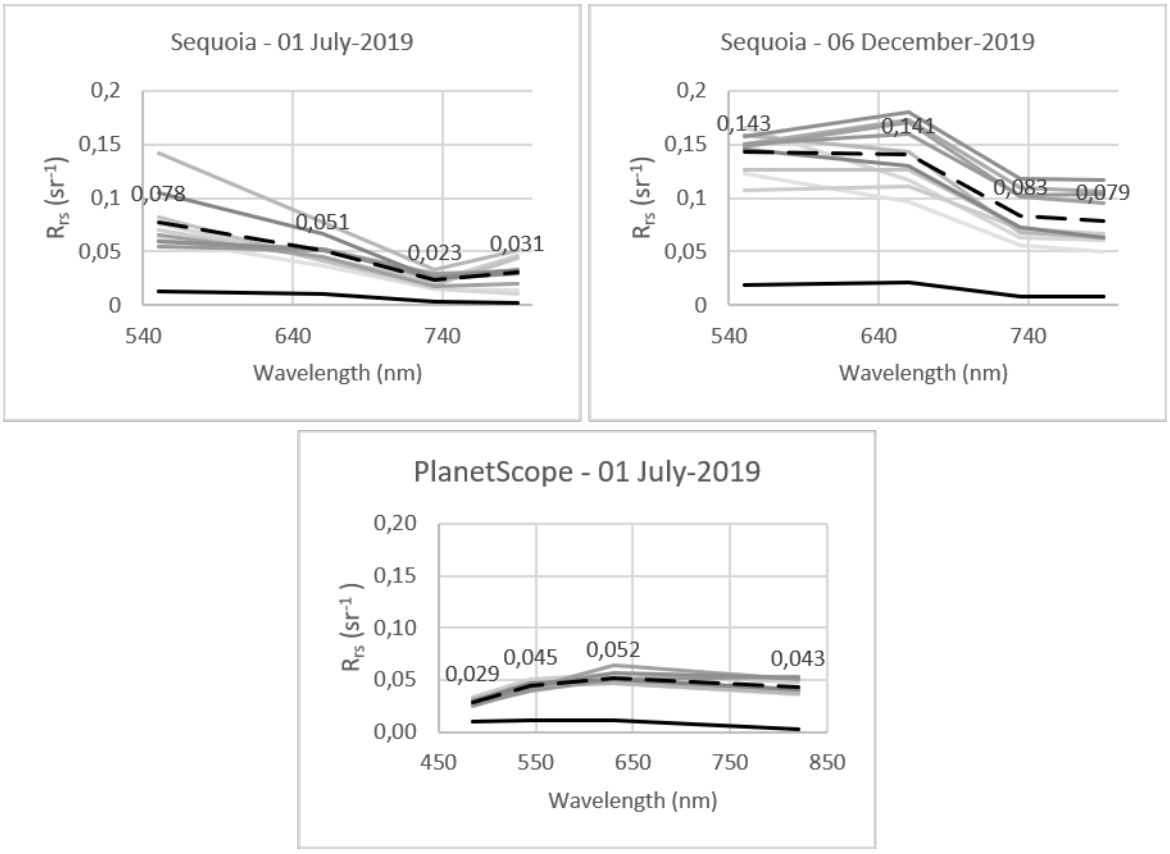

Figure 3 - R_{rs} spectra of the Sequoia and PlanetScope camera for the sample elements from the July and December field campaigns compared to the in situ R_{rs} spectrum of the average of the resampled points for the corresponding sensor and date.

Chlorophyll-a monitoring by Sequoia and Planet Airborne Sensors

Chlorophyll-a concentrations and variations in spectral responses can be empirically associated through statistical models, either by spectral indices or by individual spectral bands. These associations do not imply causality, but rather reflect the extent to which optical measurements co-vary with Chl-a concentrations under specific environmental conditions. Table 3 presents both literature-derived models and models developed from individual bands of the tested sensors. The results are expressed in terms of the coefficients of determination (R^2) and Pearson's correlation coefficient (r), highlighting the strength of the observed relationships.

After several adjustments, the best results were achieved with empirical models that utilize individual bands for both sensors. When analyzed separately, the bands exhibited different performance levels, with greater consistency observed in the PlanetScope (PS) sensor data (Maciel et al., 2020) and Sequoia (Olivetti et al., 2020). In contrast, the literature-derived models showed only moderate or no correlation. Furthermore, other models were evaluated—such as the Surface Algal Bloom Index (SABI) (Alawadi, 2010), the 3BDA-like index (KIVU) (Brivio et al., 2001), and the Kab1 and Kab2 models (Kabbara et al., 2008)—but their performance did not meet expectations.

The poor correlation observed when applying these indices can be attributed to the model's tendency to amplify errors when using sensors with low signal-to-noise ratios (SNR), particularly at low Rrs values (Jorge et al., 2017). Moreover, algorithmic approaches may result in inaccurate Chl-a estimates in turbid and eutrophic waters (Binding et al., 2020), unless the analysis specifically targets the red and near-infrared regions of the spectrum (Gilerson et al., 2010).

Table 3 Literature models and single bands of Sequoia and PlanetScope R_{rs} for Chl-a concentration retrieval

Models	Sequoia		Planet		Reference
	r	**R^2**	***r***	**R^2**	
B	-	-	0.72	0.52	-
G	x	x	**0.81**	**0.65**	-
R	**0.89**	**0.80**	0.72	0.52	-
RE	0.92	0.85	-	-	-
NIR	0.93	0.86	0.80	0.64	-
NDVI = (NIR-R)/(NIR+R)	0.67	0.45	0.71	0.51	(Lissner and Guasselli 2013); (Rouse et al. 1973)
NDCI = (RE-R)/(RE+R)	x	x	0.71	0.51	(Mishra and Mishra 2012)
RAVI = G/R	x	x	x	x	(Coelho et al. 2012)
NRAVI = (G-R)/(G+R)	0.64	0.41	x	x	(Coelho et al. 2012)
G/B	-	-	x	x	(Turner 2010)
B/R	-	-	x	x	(Mancino et al. 2009)
NIR/R	0.69	0.47	0.70	0.50	(Duan et al. 2007)
Log B/log R	-	-	x	x	(Han and Jordan 2005)
(B-R)/G	-	-	x	x	(Mayo et al. 1995)
Log (G/R)	0.64	0.41	x	x	(Hellweger et al. 2004)
Log(R/B)	-	-	x	x	(Gitelson et al. 1996)

'-': data does not exist, as the Sequoia product does not have a blue band or Planet Product does not have a red red-edge band; *x:* omitted data, as there was no correlation.

The selection of models was based on an analysis of the correlation between the tested models and the measured Chl-a concentrations. Accordingly, the empirical linear regression model for estimating Chl-a (Figure 4) from Sequoia data utilized the red spectral band (640–680 nm), while for the PlanetScope sensor, the green band (500–590 nm) produced better results. However, PlanetScope presented a lower overall performance compared to Sequoia.

Before presenting the regression results, it is important to note that the Sequoia dataset included only 10 samples (N = 10), which reduces statistical power and increases uncertainty in the regression estimates. Therefore, these results should be interpreted with caution, and further studies with larger sample sizes are recommended.

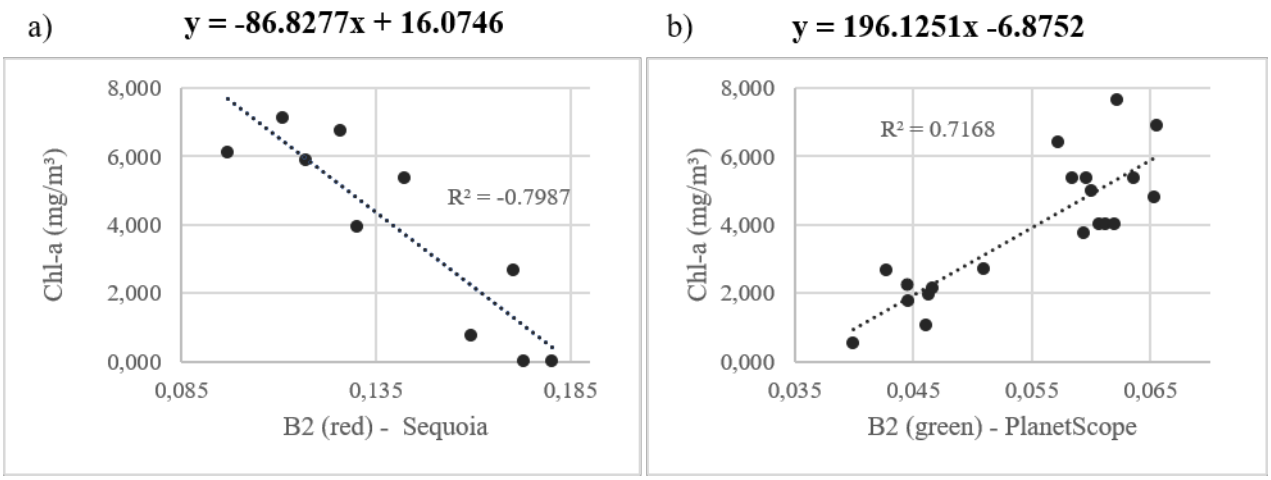

Figure 4 – Scatter plots of Chl-a estimation models of PlanetScope, and the RPA and Sequoia system

Analyzing the graphs in Figure 4, a strong negative statistical correlation was identified for the red band of Sequoia. This empirical relationship aligns with the known absorption of electromagnetic radiation by Chl-a in the red region (Chen et al., 2013). Nonetheless, it is important to note that reflectance patterns in this spectral range can also be influenced by other optically active components, particularly suspended solids, which affect backscattering and may confound the correlation (Giardino et al., 2017).

Therefore, the regression model should be interpreted as a statistical proxy for Chl-a variability rather than a direct causal mechanism, and its performance is conditioned by the optical complexity of the water body

Similar to established models, PlanetScope data showed a strong correlation with the green band, which is commonly used in models for environments with low Chl-a concentrations (Matthews, 2017), as it corresponds to the band with the highest reflectance intensity under these conditions.

Table 4 presents the validation of the Sequoia model using the jackknife method, showing that Chl-a concentrations fall within the established confidence intervals, indicating good model accuracy. The table also includes the validation of the PlanetScope model, performed through the independent extraction of three points from the original dataset. Additionally, both models were evaluated using Student's t-test, which assessed the regression coefficient and rejected the null hypothesis (H_0) at a 95% confidence level. A p-value below 5% further confirmed the rejection of H_0, indicating a linear relationship between the x and y variables. Based on these validations, the models were applied to generate Chl-a concentration maps for both sensors.

Table 4 Validation of the estimation models of Chlorophyll-a Sequoia and PlanetScope

Confidence intervals for the estimation model of Chlorophyll-a Sequoia, from the validation models with the application of the *jackknife* method.

Excluded sample element	Validation models Chla = β (B2) + α	B2 (R) 640-680 nm	Chl-a observed (mg/m³)	Chl-a estimated by the validation model (mg/m³)	Confidence Interval (CI)	
					Lim Inf.	Lim Sup.
P1	Chla = -100.83x + 18.286	0.097	6.110	8.521	-1.145	18.186
P2	Chla = -86.902x + 16.087	0.117	5.881	5.905	-4.791	16.602
P3	Chla = -83.354x + 15.498	0.111	7.128	6.247	-4.278	16.771
P4	Chla = -83.205x + 15.379	0.126	6.753	4.898	-4.649	14.446
P5	Chla = -87.273x + 15.954	0.143	5.346	3.514	-6.387	13.416
P6	Chla = -80.927x + 15.382	0.173	0.000	1.373	-11.200	13.946
P7	Chla = -93.925x + 16.893	0.171	2.673	0.877	-10.904	12.658
P8	Chla = -82.553x + 15.645	0.159	0.764	2.483	-8.444	13.410
P9	Chla = -83.599x + 15.682	0.180	0.000	0.616	-13.412	14.644
P10	Chla = -88.159x + 16.357	0.130	3.931	4.884	-5.606	15.374

Confidence intervals and RMSE for validation of the PlanetScope Chlorophyll-a estimation model, from the Chl-a concentrations of points not belonging to the model.

It should be emphasized that all models presented in this study are empirical and correlation-based, and therefore should not be interpreted as evidence of causality between spectral reflectance and Chl-a concentrations. Reflectance values in specific bands are affected simultaneously by multiple optically active components, including phytoplankton pigments, suspended solids, and colored dissolved organic matter. The regression models applied here thus provide proxies of Chl-a variability under the specific optical conditions of the study area. This distinction is critical to ensure a rigorous interpretation of the results and is consistent with the empirical nature of most remote sensing approaches in optically complex inland waters.

Spatial distribution of chlorophyll-a

The spatial distribution of Chl-a concentrations estimated by the Sequoia model (Figure 5(a)) closely aligns with the in situ limnological and spectral data of the area. In Figure 5, lower Chl-a concentrations are observed near the two effluent channels of the Riacho Fundo stream, likely due to the input of suspended solids from the stream in this region (Miguel et al., 2017) and the nutrient retention effect of Riacho Fundo's Wetland, which helps control eutrophication (Dias and Baptista, 2015). Additionally, water currents from the Riacho Fundo stream, particularly following intense rainfall, may have contributed to phytoplankton dispersion.

It is likely that the currents from Channel 1, which have a greater flow, create the boundary between the area near the ETE Sul (where group 1 samples are located) and the rest of the area (group 2). In Channel 2, to the east, a more distinct boundary is observed where water rapidly changes its configuration, possibly due to convective movements, with cooler Wetland water sinking when it meets warmer lake water in deeper areas (Leite and Baptista, 2016). Between the two channels, Chl-a concentrations are absent, likely due to filtration through the Wetland combined with sediment input from both channels.

Near the ETE Sul, a gradual change in Chl-a concentrations can be attributed to the combined effluents from the ETE and Riacho Fundo stream through Channel 1. Higher concentrations are observed near the ETE Sul and in group 2, farther from the Riacho Fundo effluent, correlating with elevated nutrient inputs from the ETE Sul, identified as the primary source of organic material in the region (Dias, 2017).

Figure 5(c) displays the spatial and temporal distributions of Chl-a concentrations based on PlanetScope data for May, July, September, and October 2019. In May, a darker region west of Channel 1 likely indicates high concentrations of Colored Dissolved Organic Matter (CDOM), which can enter through storm sewers and ETE Sul effluent (Dias, 2017). Excess CDOM reduces sunlight penetration, limiting phytoplankton photosynthesis and masking Chl-a spectral signals (Mannino et al., 2008), compounded by suspended solids from Riacho Fundo. Higher organic matter concentrations also reduce reflectance in the blue and green spectral regions (<600 nm) (Bukata et al., 2018), potentially influencing the Chl-a PS map derived from the green band (centered at 545 nm).

The PS maps for July, September, and October correspond to drought periods with minimal rainfall. Both July and September images show a noisy appearance, likely due to different PS nanosatellite acquisitions and low SNR sensors (Traganos et al., 2017). The October image may have been affected by specular reflection, impacting the Chl-a estimate. Despite these challenges, the larger sample size and seasonal coverage of PS data enabled the model to effectively map Chl-a spatial distribution, consistent with the region's limnological characteristics, particularly during the rainy season.

Comparison of applied methods

When comparing RPA and satellite-based remote sensing platforms for Chl-a estimation, it is crucial to consider not only spatial, spectral, and temporal resolution, but also biomass concentration, operational feasibility, and sensor performance under varying environmental conditions (Greb et al., 2018).

While PlanetScope sensors offer high temporal resolution and broad spatial coverage (Mansaray et al., 2021), their broader spectral bands and lower signal-to-noise ratio (SNR) can limit the detection of low chlorophyll concentrations, particularly in clear or oligotrophic waters where backscatter is low and chlorophyll-a absorption is subtle, often below the sensitivity threshold of standard satellite sensors (Jorge et al., 2017).

In contrast, RPA systems equipped with multispectral sensors, such as Sequoia, have demonstrated high accuracy in small-scale studies, especially in moderately to highly turbid environments.

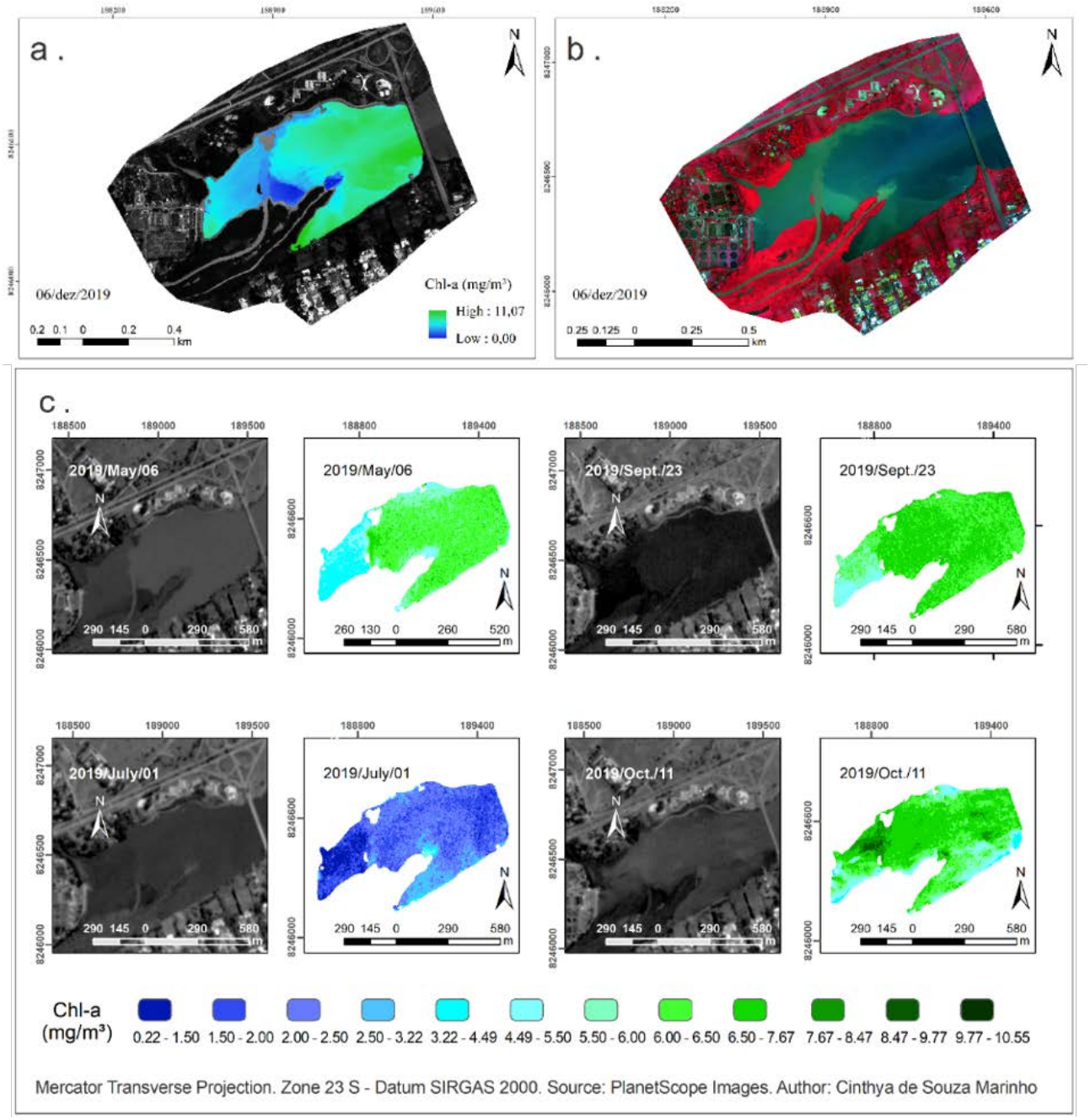

Figure 5 - Spatial distribution of Chl-a concentrations (mg/m³) in the mouth of Riacho Fundo. **a-b** from Sequoia's Chl-a estimation model as of December 6, 2019. **a.** Chl-a estimated from the linear relation with the red band (640-680 nm) of Sequoia**. b.** Sequoia's R4G2B1 color composition, for a better perspective of the aquatic environment in the day. **c.** from the Chl-a PlanetScope estimate model on 06/May/2019, 01/July/2019, 23/Sep/2019 and 11/Oct/2019. On the right, estimated Chl-a. On the left, R3G2B1 true color composites of PlanetScope products

For instance, Zhao et al. (2023) successfully estimated Chl-a concentrations ranging from 10 to 40 µg/L using regression models applied to UAV multispectral imagery. Their study highlighted the advantage of narrow-band sensors and flexible flight planning, allowing synchronization with environmental events such as blooms or runoff pulses.

Spectral resolution sensor's ability to distinguish between wavelengths is an important factor. RPA sensors like Sequoia have narrower spectral bands (10–40 nm), enabling precise differentiation of specific water constituents. In contrast, orbital sensors such as PlanetScope have broader bands (60–90 nm), which can limit sensitivity and specificity.

Additionally, Irie et al. (2024) emphasized the importance of turbidity correction in UAV-based models, which significantly improved Chl-a estimation accuracy in reservoirs (R^2 = 0.84). Recent reviews (Kumar et al., 2025) confirm that satellites are ideal for long-term synoptic monitoring, while UAVs provide high-resolution detail and adaptability for near-real-time mana-

gement and targeted monitoring in eutrophic and mesotrophic systems.

RPA systems also offer advantages for monitoring small or difficult-to-access areas, such as tributary channels, which are critical for assessing nutrient and constituent flows into reservoirs. RPAs are particularly suitable during the rainy season. However, small RPAs are less practical for large-scale monitoring, such as covering the entirety of Paranoá Lake, due to extended flight times, battery limitations, and increased image processing requirements.

Both RPA and satellite systems generated Chl-a estimation maps consistent with the limnological and meteorological characteristics of the study area during the rainy season. Dry season predictions were less reliable, likely due to reduced reflectance intensity and lower optical signal, particularly in clearer waters. Despite these limitations, both platforms produced validated Chl-a estimation models applicable to the study area. Thus, the choice of platform should be guided by the required spatial detail, area extent, and seasonal conditions.

CONCLUSIONS

This study contributes to the geosciences by providing a comparative assessment of chlorophyll-a (Chl-a) estimation techniques using remote sensing data from both Remotely Piloted Aircraft (RPA) and high-resolution satellite (PlanetScope) sensors in inland aquatic environments. By evaluating the spatial, spectral, and temporal performance of each platform under varying environmental and trophic conditions, the research reinforces the relevance of integrated remote sensing approaches for monitoring water quality, particularly in areas subject to diffuse and point-source pollution. Both RPA systems and high spatial resolution orbital platforms can provide valuable information for monitoring smaller areas, such as tributary channels.

The PlanetScope and RPA equipped with a Sequoia camera successfully enabled Chl-a estimation over a 38-hectare area, identifying regions influenced by varying pollution sources. The RPA system was able to generate a model for Chl-a estimation during the rainy season, likely due to higher concentrations of optically active components (OACs) resulting in increased reflectance intensity. In contrast, the PlanetScope system allowed Chl-a estimates for both rainy and dry seasons, leveraging data from multiple periods and a larger number of sampling points. However, neither system produced strong correlations with Chl-a or field spectroradiometry when only dry season data were considered, likely due to low backscatter in clear waters affecting the remote sensing reflectance (Rrs).

Despite the advantages of high spatial resolution, limitations in signal-to-noise ratio (SNR) constrained the effective use of reflectance information. Additionally, low overall Chl-a concentrations and the sampling design posed statistical challenges, limiting the certainty of the models' predictions.

Hydrological and anthropogenic factors strongly influenced Chl-a distribution. The Riacho Fundo stream contributes significant sediment input, modifying spectral responses near the water inlet and affecting spatial Chl-a patterns, particularly during the rainy season. The ETE Sul, storm sewers, and potential clandestine discharges are likely the main sources of nutrients, promoting phytoplankton development in the area.

The study also highlights key limitations for Chl-a detection in oligotrophic waters, such as low reflectance intensity and weak correlations during dry periods. These findings underscore the need for methodological improvements, including:

(i) increasing the number of ground-truth samples,

(ii) enhancing atmospheric and radiometric corrections,

(iii) incorporating machine learning models to improve sensitivity at low Chl-a levels, and

(iv) using spectral indices tailored to specific environmental contexts.

Future work should focus on expanding multi-seasonal datasets, integrating UAV and satellite data with in situ observations, and refining bio-optical models to improve the accuracy and operational use of Chl-a remote sensing in freshwater systems. As a result, this approach supports better-informed decision-making in water resource management and contributes to the advancement of remote sensing applications in geosciences.

REFERENCES

ADADE, R.; AIBINU, A.M.; EKUMAH, B.; ASAANA, J. Unmanned Aerial Vehicle (UAV) applications in coastal zone management—a review. **Environmental Monitoring and Assessment**, v. 193, 154, 2021. https://doi.org/10.1007/s10661-021-08949-8

ALAWADI, F. Detection of surface algal blooms using the newly developed algorithm surface algal bloom index (SABI). In: REMOTE SENSING OF THE OCEAN, SEA ICE, AND LARGE WATER REGIONS, 2010. *Proceedingv…* ISOP: 2010, v. 7825, p. 1–14,

APHA; AWWA; WEF. **Standard Methods for the Examination of Water and Wastewate***r*. 23. ed. New York: American Public Health Association, 2017.

ASTUTI, I.S.; MISHRA, D.R.; MISHRA, S.; SCHAEFFER, B. Spatio-temporal dynamics of inherent optical properties in oligotrophic northern Gulf of Mexico estuaries. **Continental Shelf Research**, v. 166, p. 92–107, 2018. https://doi.org/10.1016/j.csr.2018.06.016

BATISTA, B.D. & FONSECA, B.M. Phytoplankton in the central region of Paranoá Lake, Federal District of Brazil: an ecological and sanitary approach. **Engenharia Sanitária e Ambiental**, v. 23, n. 2, p. 229-241, 2018. https://dx.doi.org/10.1590/s1413-41522018169124

BINDING, C.E.; STUMPF, R.P.; SHUCHMAN, R.A.; SAYERS, M.J. Advances in Remote Sensing of Great Lakes Algal Blooms. In: CROSSMAN, J.; WEISENER, C. (eds.). **Contaminants of the Great Lakes**. Cham: Springer, 2020. The Handbook of Environmental Chemistry, v. 101. https://doi.org/10.1007/698_2020_589

BRAZIL. **Ministério do Meio Ambiente. Conselho Nacional do Meio Ambiente** – CONAMA. Resolução n. 357, de 17 de março de 2005.

BRIVIO, P.A.; GIARDINO, C.; ZILIOLI, E. Determination of chlorophyll concentration changes in Lake Garda using an image-based radiative transfer code for Landsat TM images. **International Journal of Remote Sensing**, v. 22, p. 487-502, 2001. https://doi.org/10.1080/014311601450059

BUKATA, R.P.J.; KOONDRATYEV, K.Y.; POZOZDNYAKOV, D.V. **Optical properties and remote sensing of inland and coastal waters**. Boca Raton: CRC Press, 362 p., 2018.

CABALLERO, I.; FERNÁNDEZ, R.; ESCALANTE, O.M.; MAMÁN, L.; NAVARRO, G. New capabilities of Sentinel-2A/B satellites combined with in situ data for monitoring small harmful algal blooms in complex coastal waters. **Scientific Reports**, v. 10, p. 8743, 2020. https://doi.org/10.1038/s41598-020-65600-1

CEOS – COMMITTEE ON EARTH OBSERVATION SATELLITES. DEKKER, A. G.; PINNEL, N. (eds.). **Feasibility study for an aquatic ecosystem Earth observing system**. Report v. 2.0. CSIRO, Canberra, ACT, Australia, 2018.

CHEN, J.; ZHANG, M.; CUI, T.; WEN, Z. A review of some important technical problems in respect of satellite remote sensing of chlorophyll-a concentration in coastal waters. **IEEE Journal of Selected Topics in Applied Earth Observations and Remote Sensing**, v. 6, n. 5, p. 2275-2289, 2013. https://doi.org/10.1109/JSTARS.2013.2242845

CHENG, K.H.; CHAN, S.N.; LEE, J.H.W. Remote sensing of coastal algal blooms using unmanned aerial vehicles (UAVs). **Marine Pollution Bulletin**, v. 152, 110889, 2020. https://doi.org/10.1016/j.marpolbul.2020.110889

CICERELLI, R. E.; GALO, M. L. B. T. Multisource remote sensing applied to the detection of phytoplankton in inland waters. **Revista Brasileira de Engenharia Agrícola e Ambiental**, v. 19, n. 3, p. 259-265, 2015.

CODEPLAN – COMPANHIA DE PLANEJAMENTO DO DISTRITO FEDERAL. **Atlas do Distrito Federal.** Brasília: GDF, 78 p., 1984.

COELHO, L.; ROCHE, K. F.; PARANHOS FILHO, A. C.; LEMOS, V. B. Uso do sensor CBERS/CCD na avaliação do estado trófico do reservatório Lago do Amor (Campo Grande, MS). **Revista Brasileira de Cartografia**, v. 63, n. 2, 2012.

DARVISHZADEH, R.; SKIDMORE, A.; SCHLERF, M.; ATZBERGER, C. Inversion of a radiative transfer model for estimating vegetation LAI and chlorophyll in a heterogeneous grassland. **Remote Sens. Environ.**, v. 112, n. 5, p. 2592–2604, 2008.

DASH, J.; OGUTU, B. O. Recent advances in space-borne optical remote sensing systems for monitoring global terrestrial ecosystems. **Progress in Physical Geography**, v. 40, n. 2, p. 322–351, 2016. https://doi.org/10.1177/0309133316639403

DE ALMEIDA, T.; CICERELLI, R.E.; ROIG, H.L.; BAPTISTA, G.; NEUMANN, M.R.B. Delineamento amostral no monitoramento de reservatório de uso múltiplo utilizando reflectância acumulada em imagens Landsat 8. **Sustainability, Agri, Food and Environmental Research-DISCONTINUED**, v. 6, n. 3, p. 28-35, 2018.

DE AQUINO, I.G.; ROIG, H.L.; OLIVEIRA, E.S.; GARNIER, J.; GUIMARÃES, E.M.; KOIDE, S. Temporal variation of suspended sediments and mineralogy using an improved automatic sampler system in the Riacho Fundo Stream, Brasília, Distrito Federal, Brazil. **Geol. USP, Sér. cient.**, São Paulo, v. 18, n. 2, p. 117–185, 2018.

DIAS, R.Z. & BAPTISTA, G.M.M. Wetland nutrient retention and multitemporal growth – Case study of Riacho Fundo's Wetland. **Acta Limnologica Brasiliensia**, v. 27, n. 3, p. 254–264, 2015. https://doi.org/10.1590/S2179-975X0114

DUAN, H.T.; ZHANG, Y.Z.; ZHAN, B.; SONG, K.S.; WANG, Z.M. Assessment of chlorophyll-a concentration and trophic state for Lake Chagan using Landsat TM and field spectral data. **Environmental Monitoring and Assessment**, v. 129, p. 295–308, 2007.

FINK, G.; BURKE, S.; SIMIS, S.G.H.; KANGUR, K.; KUTSER, T.; MULLIGAN, M. Management options to improve water quality in Lake Peipsi: Insights from large scale models and remote sensing. **Water Resour. Manage**., v. 34, p. 2241–2254, 2020. https://doi.org/10.1007/s11269-018-2156-5

FONSECA, F.O. **Views over Lake Paranoá. Olhares sobre o Lago Paranoá.** Brasília: Secretaria de Meio Ambiente e Recursos Hídricos, 2001.

GIARDINO, C.; BRESCIANI, M.; BRAGA, F.; CAZZANIGA, I.; DE KEUKELAERE, L.; KNAEPS, E. & BRANDO, V. E. Bio-optical modeling of total suspended solids. In: MISHRA, D. R.; OGASHAWARA, I.; GITELSON, A. A. **Bio-optical Modeling and Remote Sensing of Inland Waters.** 1st ed. Amsterdam: Elsevier, cap. 5, 2017.

GILERSON, A.A.; GITELSON, A.A.; ZHOU, J.; GURLIN, D.; MOSES, W.; IOANNOU, I.; AHMED, S.A. **Algorithms for remote estimation of chlorophyll-a in coastal and inland waters using red and near infrared bands**. Opt. Express, v. 18, n. 23, p. 24109–24125, 2010.

GITELSON, A.A.; YACOBI, Y.Z.; KARNIELI, A.; KRESS, N. Reflectance spectra of polluted marine waters in Haifa Bay, Southeastern Mediterranean: features and application for remote estimation of chlorophyll concentration. **Israel Journal of Earth Science**, v. 45, p. 127–136, 1996.

GRANDE, T.O.; ALMEIDA, T.; CICERELLI, R.E. Object-oriented classification in association with accumulated reflectance and data mining tools. **Pesq. Agropec. Bras.**, Brasília, v. 51, n. 12, p. 1983–1991, 2016. https://doi.org/10.1590/S0100-204X2016001200009

GREB, S.; DEKKER, A. G.; BINDING, C.; BERNARD, S.; BROCKMANN, C.; DIGIACOMO, P.; ... WANG, M. Earth observations in support of global water quality monitoring. **International Ocean-Colour Coordinating Group**, 2018.

GUO, H.; HUANG, JJ.; CHEN, B.; GUO, X.; SINGH, V.P. A machine learning-based strategy for estimating non-optically active water quality parameters using Sentinel-2 imagery.

International Journal of Remote Sensing, v. 42, n. 5, p. 1841–1866, 2021. https://doi.org/10.1080/01431161.2020.1846222

HAN, L. & JORDAN, K. Estimating and mapping chlorophyll a concentration in Pensacola Bay, Florida using Landsat ETM data. **International Journal of Remote Sensing**, v. 26, p. 5245–5254, 2005.

HELLWEGER, F.L.; SCHLOSSER, P.; LALL, U.; WEISSEL, J.K. Use of satellite imagery for water quality studies in New York Harbor. **Estuarine, Coastal and Shelf Science**, v. 61, n. 3, p. 437–448, 2004.

HERMUCHE, P.M. & SANO, E.E. Identificação da floresta estacional decidual no Vão do Paranã, estado de Goiás, a partir da análise da reflectância acumulada de imagens do sensor ETM+/Landsat-7. **Revista Brasileira de Cartografia**, n. 63/03, 2011.

INMET – NATIONAL INSTITUTE OF METEOROLOGY. **Technical Notes - Notas Técnicas**. Disponível em: https://portal.inmet.gov.br/notasTecnicas. Acesso em: 10 jul. 2020.

IRIE, T.; SATO, K.; TANAKA, H. Estimation method of chlorophyll concentration distribution based on UAV aerial images considering turbid water distribution in a reservoir. **Sensors**, v. 24, n. 2, 314, 2024. https://doi.org/10.3390/s24020314

IZADI, M.; SULTAN, M.; KADIRI, R. E.; GHANNADI, A.; ABDELMOHSEN, K. A remote sensing and machine learning-based approach to forecast the onset of harmful algal bloom. **Remote Sensing**, v. 13, n. 19, 3863, 2021.

JALLY, S.K.; MISHRA, A.K.; BALABANTARAY, S. Retrieval of suspended sediment concentration of the Chilika Lake, India using Landsat-8 OLI satellite data. **Environmental Earth Sciences**, v. 80, 298, 2021. https://doi.org/10.1007/s12665-021-09581-y

JAUD, M.; DELACOURT, C.; LE DANTEC, N. ; ALLEMAND, P.; AMMANN, J.; GRANDJEAN, P.; FLOC'H, F. Diachronic UAV photogrammetry of a sandy beach in Brittany (France) for a long-term coastal observatory. ISPRS **International Journal of Geo-Information**, v. 8, n. 6, 260, 2019. https://doi.org/10.3390/ijgi8060267

JORGE, D.; BARBOSA, C.; DE CARVALHO, L.; AFFONSO, A.G.; LOBO, F.D.L.; NOVO, E.M.D.M. SNR (Signal-To-Noise Ratio) impact on water constituent retrieval from simulated images of optically complex Amazon lakes. **Remote Sensing**, v. 9, n. 7, 644, 2017. https://doi.org/10.3390/rs9070644

KHAN, R. M.; SALEHI, B.; MAHDIANPARI, M.; MOHAMMADIMANESH, F.; MOUNTRAKIS, G.; QUACKENBUSH, L.J. A meta-analysis on harmful algal bloom (HAB) detection and monitoring: a remote sensing perspective. **Remote Sensing**, v. 13, n. 21, 4347, 2021.

KIRK, J.T.O. **Light & photosynthesis in aquatic ecosystems**. v. 2, Cambridge: Cambridge University Press, 507 p., 1994. http://dx.doi.org/10.1017/CBO9780511623370

KISLIK, C.; DRONOVA, I.; KELLY, M. UAVs in support of algal bloom research: a review of current applications and future opportunities. **Drones**, v. 2, n. 4, 35, 2018. http://dx.doi.org/10.3390/drones2040035

KUMAR, A.; et al. Remote sensing of cyanobacterial harmful algal blooms: current trends and future directions. **Progress in Environmental Geography**, v. 4, n. 1, p. 131–150, 2025.

KWON, Y. S.; PYO, J.; KWON, Y.H.; DUAN, H.; CHO, K.H.; PARK, Y.Drone-based hyperspectral remote sensing of cyanobacteria using vertical cumulative pigment concentration in a deep reservoir. **Remote Sensing of Environment**, v. 236, 111517, 2020. https://doi.org/10.1016/j.rse.2019.111517

LAMPARELLI, M. C. **Trophic Status in São Paulo State water bodies: evaluation of monitoring methodologies**. São Paulo, 2004. 235 p. Tese (Doutorado) – Instituto de Biociências, Universidade de São Paulo. https://doi

LAN, J.; LIU, P.; HU, X.; ZHU, S. Harmful algal blooms in eutrophic marine environments: causes, monitoring, and treatment. **Water**, v. 16, n. 17, p. 2525, 2024.

LEE, S.; EOM, J.; SYIFA, M.; PARK, S. J.; PARK, Y. C.; LEE, C. W. Assessing the effects of external factors on sediment erosion and accumulation in an estuarine environment based on images from unmanned aerial vehicles: Namdaecheon, **South Korea**. Geosci. J., v. 25, p. 547–559, 2021. https://doi.org/10.1007/s12303-021-0011-9

LEITE, B. & BAPTISTA, G. Evaluation of the Environmental Importance of Riacho Fundo's Wetland to Paranoa Lake and Neighboring Communities. **Rev. Bras. Geogr. Fís.**, v. 8, n. 5, p. 1524-1540, 2016. https://doi.org/10.5935/1984-2295.20150085

LISSNER, J.B. & GUASSELLI, L.A. Variations of the Normalized Difference Vegetation Index (NDVI) in the Itapeva-RS lake, north coast of Rio Grande do Sul, Brazil, from temporal series analysis. **Soc. Nat.**, v. 25, n. 2, p. 427-440, 2013. https://doi.org/10.1590/S1982-45132013000200016

LIU, H.; PAN, D.; ZHU, M.; ZHANG, D. Occurrence and emergency response of 2-Methylisoborneol and Geosmin in a large shallow drinking water reservoir. **Clean Soil, Air, Water,** v. 44, n. 1, p. 63-71, 2016. https://doi.org/10.1002/clen.201500077

LOBO, F.D.L.; NAGEL, G.W.; MACIEL, D.A.; CARVALHO, L.A.S.D.; MARTINS, V.S.; BARBOSA, C.C.F.; NOVO, E. M.L.D.M. AlgaeMAp: Algae bloom monitoring application for inland waters in Latin America. **Remote Sensing**, v. 13, n. 15, 2874, 2021.

LU, S.; DENG, R.; LIANG, Y.; XIONG, L.; AI, X.; QIN, Y. Remote sensing retrieval of total phosphorus in the Pearl River channels based on the GF-1 remote sensing data. **Remote Sens.**, v. 12, n. 9, 1420, 2020. http://dx.doi.org/10.3390/rs12091420

MACHADO, M.T.S.M. & BAPTISTA, G.M.M. Remote sensing as a tool for monitoring Paranoá Lake's water quality (Brasília, Brazil). **Engenharia Sanitária e Ambiental**, Rio de Janeiro, v. 21, n. 2, p. 357-365, jun. 2016. https://doi.org/10.1590/S1413-41522016141970

MACIEL, D.A.; BARBOSA, C.C.F.; DE MORAES NOVO, E.M.L.; PAHLEVAN, N.; BONNET, M.P.; DE SOUZA PAULINO, R.; MARTINS, V. **Water transparency trends in Amazon Basin from long-term Landsat data**, 2023.

MACIEL, D.A.; NOVO, E.M.L.D.M.; BARBOSA, C.C.F.; MARTINS, V.S.; FLORES JÚNIOR, R.; OLIVEIRA, A.H.; LOBO, F.D.L. Evaluating the potential of CubeSats for remote sensing reflectance retrieval over inland waters. **International Journal of Remote Sensing**, v. 41, n. 7, p. 2807-2817, 2020. https://doi.org/10.1080/2150704X.2019.1697003

MACIEL, D.; NOVO, E.; SANDER DE CARVALHO, L.; BARBOSA, C.; FLORES JÚNIOR, R.; DE LUCIA LOBO, F. Retrieving total and inorganic suspended sediments in Amazon floodplain lakes: a multisensor approach. **Remote Sensing**, v. 11, n. 15, p. 1744, 2019. http://dx.doi.org/10.3390/rs11151744

MANCINO, G.; NOLÈ, A.; URBANO, V.; AMATO, M.; FERRARA, A. Assessing water quality by remote sensing in small lakes: the case study of Monticchio lakes in southern Italy. **iForest**, v. 2, p. 154-161, 2009. https://doi.org/10.3832/ifor0507-002

MANNINO, A.; RUSS, M.E.; HOOKER, S.B. Algorithm development and validation for satellite derived distributions of DOC and CDOM in the U.S. Middle Atlantic Bight. J**ournal of Geophysical Research**, v. 113, C07051, 2008.

MANSARAY, A.S.; DZIALOWSKI, A.R.; MARTIN, M.E.; WAGNER, K.L.; GHOLIZADEH, H.; STOODLEY, S.H. Comparing PlanetScope to Landsat-8 and Sentinel-2 for sensing water quality in reservoirs in agricultural watersheds. **Remote Sensing,** v. 13, n. 9, p. 1847, 2021.

MAR DA COSTA, N. Y.; BOAVENTURA, G. R.; MULHOLLAND, D. S.; ARAÚJO, D. F.; MOREIRA, R.C.; FAIAL, K.C.; BOMFIM, E.D.O. Biogeochemical mechanisms controlling trophic state and micropollutant concentrations in a

tropical artificial lake. **Environmental Earth Sciences**, v. 75, p. 854, 2016. https://doi.org/10.1007/s12665-016-5629-y

MARKOGIANNI, V.; KALIVAS, D.; PETROPOULOS, G.P.; DIMITRIOU, E. Estimating Chlorophyll-a of inland water bodies in Greece based on Landsat data. **Remote Sensing**, v. 12, n. 13, p. 2087, 2020. http://dx.doi.org/10.3390/rs12132087

MARTINEZ, J.M.; ESPINOZA-VILLAR, R.; ARMIJOS, E.; SILVA MOREIRA, L. The optical properties of river and floodplain waters in the Amazon River Basin: implications for satellite-based measurements of suspended particulate matter - Supplementary material. **Journal of Geophysical Research: Earth Surface**, v. 1, n. 860, p. 1–11, 2015.

MATTHEWS, M.W. Bio-optical modeling of phytoplankton chlorophyll-a. In: MISHRA, D.R.; OGASHAWARA, I.; GITELSON, A. A. (Eds.). **Bio-optical Modeling and Remote Sensing of Inland Waters**. 1st ed. Elsevier, 2017. Cap. 6.

MAYO, M.; GITELSON, A.; YACOBI, Y.Z.; BEN-AVRAHAM, Z. Chlorophyll distribution in Lake Kinneret determined from Landsat Thematic Mapper data. **International Journal of Remote Sensing**, v. 16, p. 175–182, 1995.

MIGUEL, R.; ROIG, H.L.; OLIVEIRA, E.S. Analysis of the silting process in the Riacho Fundo arm of Lake Paranoá - DF, using geoprocessing and sedimentometry techniques. In: SIMPÓSIO DE GEOLOGIA DO CENTRO OESTE, XV, 2017, Goiânia. *Anais*... Goiânia: Sociedade Brasileira de Geologia – Núcleo Centro-Oeste, 2017. p. 180-185.

MISHRA, D.R.; MISHRA, S.; NARUMALANI, S. Hyperspectral remote sensing of cyanobacteria: successes and challenges. Proc. SPIE 9263, **Multispectral, Hyperspectral, and Ultraspectral Remote Sensing Technology, Techniques and Applications V**, 92630J, 2014. https://doi.org/10.1117/12.2069320

MISHRA, S. & MISHRA, D. R. Normalized difference chlorophyll index: a novel model for remote estimation of chlorophyll-a concentration in turbid productive waters. **Remote Sensing of Environment**, v. 117, p. 394–406, 2012. https://doi.org/10.1016/j.rse.2011.10.016

MOBLEY, C.D. Estimation of the remote-sensing reflectance from above-surface measurements. **Applied Optics**, v. 38, n. 36, p. 7442–7455, 1999.

MORETTIN, P.A. & BUSSAB, W. O. **Basic Statistics – Estatística Básica**. 5. ed. São Paulo: Saraiva, 2002. 526 p. ISBN 8502034979.

NGWENYA, N.; BANGIRA, T.; SIBANDA, M.; KEBEDE GURMESSA, S.; MABHAUDHI, T. UAV-based remote sensing of chlorophyll-a concentrations in inland water bodies: a systematic review. **Geocarto International**, v. 40, n. 1, p. 2452-246, 2025.

OGASHAWARA, I.; MISHRA, D.R.; GITELSON, A.A. Remote sensing of inland waters: background and current state-of-the-art. In: MISHRA, D. R.; OGASHAWARA, I.; GITELSON, A. A. **Bio-optical Modeling and Remote Sensing of Inland Waters**. 1st ed. Elsevier, 2017. Cap. 1.

OLIVETTI, D.; CICERELLI, R.; MARTINEZ, J.M.; ALMEIDA, T.; CASARI, R.; BORGES, H.; ROIG, H. Comparing unmanned aerial multispectral and hyperspectral imagery for harmful algal bloom monitoring in artificial ponds used for fish farming. **Drones**, v. 7, n. 7, p. 410, 2023.

OLIVETTI, D.; ROIG, H.; MARTINEZ, J.M.; BORGES, H.; FERREIRA, A.; CASARI, R.; MALTA, E. Low-cost unmanned aerial multispectral imagery for siltation monitoring in reservoirs. **Remote Sensing**, v. 12, n. 11, p. 1855, 2020.

ORTEGA-TEROL, D.; HERNANDEZ-LOPEZ, D.; BALLESTEROS, R.; GONZALEZ-AGUILERA, D. Automatic hotspot and sun glint detection in UAV multispectral images. **Sensors**, v. 17, n. 10, p. 1–16, 2017.

PAHLEVAN, N.; SMITH, B.; SCHALLES, J.; BINDING, C.; CAO, Z.; MA, R.; STUMPF, R. Seamless retrievals of chlorophyll-a from Sentinel-2 (MSI) and Sentinel-3 (OLCI) in inland and coastal waters: a machine-learning approach. **Remote Sensing of Environment**, v. 240, p. 111604, 2020. ISSN 0034-4257. https://doi.org/10.1016/j.rse.2019.111604

PAHLEVAN, N.; WEI, J.; SCHAAF, C. B.; SCHOTT, J. R. Evaluating radiometric sensitivity of Landsat 8 over coastal/inland waters. Report GSFC-E-DAA-TN17807, **International Geoscience and Remote Sensing Symposium** (IGARSS), 2014.

PAPENFUS, M.; SCHAEFFER, B.; POLLARD, A.I.; LOFTIN, K. Exploring the potential value of satellite remote sensing to monitor chlorophyll-a for US lakes and reservoirs. **Environmental Monitoring and Assessment**, v. 192, p. 808, 2020. https://doi.org/10.1007/s10661-020-08631-5

PARROT. **Parrot Sequoia User Manual.** Disp.: https://www.manualslib.com/products/Parrot-Sequoia-6911496.html. Acesso em: 10 jun. 2019.

PEPPA, M.; VASILAKOS, C.; KAVROUDAKIS, D. Eutrophication monitoring for Lake Pamvotis, Greece, using Sentinel-2 data. **ISPRS International Journal of Geo-Information**, v. 9, n. 3, p. 143, 2020. http://dx.doi.org/10.3390/ijgi9030143

PEREIRA-SANDOVAL, M.; URREGO, E.P.; RUIZ-VERDÚ, A.; TENJO, C.; DELEGIDO, J.; SORIA-PERPINYÀ, X.; MORENO, J. Calibration and validation of algorithms for the estimation of chlorophyll-a concentration and Secchi depth in inland waters with Sentinel-2. **Limnetica**, v. 38, n. 1, p. 471–487, 2019. https://dx.doi.org/10.23818/limn.38.27

PLANET. **Planet Imagery Product Specifications.** Disponível em: https://assets.planet.com/docs/Planet_Combined_Imagery-Product_Specs_letter_screen.pdf. Acesso em: 10 jun. 2020.

PRICE, J.I. & HEBERLING, M.T. The effects of source water quality on drinking water treatment costs: a review and synthesis of empirical literature. **Ecological Economics**, v. 151, p. 195–209, 2018. https://doi.org/10.1016/j.ecolecon.2018.04.014

ROLIM, S.B.A.; VEETTIL, B.K.; VIEIRO, A.P.; KESSLER, A.B.; GONZATTI, C. Remote sensing for mapping algal blooms in freshwater lakes: a review. **Environmental Science and Pollution Research**, v. 30, n. 8, p. 19602–19616, 2023.

ROTTA, L.H.; ALCÂNTARA, E.H.; WATANABE, F.S.; RODRIGUES, T.W.; IMAI, N.N. Atmospheric correction assessment of SPOT-6 image and its influence on models to estimate water column transparency in tropical reservoir. **Remote Sensing Applications: Society and Environment**, v. 4, p. 158–166, 2016. http://dx.doi.org/10.1016/j.rsase.2016.09.001

ROUSE JR., J.W.; HAAS, R.H.; DEERING, D.W.; SCHELL, J.A.; HARLAN, J. C. Monitoring the vernal advancement and retrogradation (green wave effect) of natural vegetation. Progress Report RSC 1978-1, **Remote Sensing Center**, Texas A&M Univ., College Station, 93 p., 1973.

SABERIOON, M.; BROM, J.; NEDBAL, V.; SOUČEK, P.; CÍSAŘ, P. Chlorophyll-a and total suspended solids retrieval and mapping using Sentinel-2A and machine learning for inland waters. **Ecological Indicators**, v. 113, 106236, 2020. https://doi.org/10.1016/j.ecolind.2020.106236

SCHALLES, J.F. & YACOBI, Y.Z. Remote detection and seasonal patterns of phycocyanin, carotenoid and chlorophyll-a pigments in eutrophic waters. Archive Hydrobiologia. Special Issues Adv. **Limnological**, v. 55, p. 153–168, 2020.

SHANG, S.; LEE, Z.; LIN, G.; HU, C.; SHI, L.; ZHANG, Y.; YAN, J. Sensing an intense phytoplankton bloom in the western Taiwan Strait from radiometric measurements on a UAV. **Remote Sensing of Environment**, v. 198, p. 85–94, 2017.

SÒRIA-PERPINYÀ, X.; VICENTE, E.; URREGO, P.; PEREIRA-SANDOVAL, M.; RUÍZ-VERDÚ, A.; DELEGIDO, J.; MORENO, J. Remote sensing of cyanobacterial blooms in a hypertrophic lagoon (Albufera of València, Eastern Iberian Peninsula) using multitemporal Sentinel-2 images. **Science of the Total Environment,** v. 698, 134305, 2020. https://doi.org/10.1016/j.scitotenv.2019.134305

TESFAYE, A. Remote sensing-based water quality parameters

retrieval methods: a review. **East African Journal of Environment and Natural Resources**, v. 7, n. 1, p. 80–97, 2024.

TRAGANOS, D.; CERRA, D.; REINARTZ, P. Cubesat-derived detection of seagrasses using Planet imagery following unmixing-based denoising: is small the next big? **International Archives of Photogrammetry, Remote Sensing and Spatial Information Sciences**, XLII-1/W1, p. 283–287, 2017. https://doi.org/10.5194/isprs-archives-XLII-1-W1-283-2017

TUNDISI, J.G.; MATSUMURA-TUNDISI, T.; ARANTES JUNIOR, J.D.; TUNDISI, J.E.M.; MANZINI, N.F.; DUCROT, R. The response of Carlos Botelho (Lobo, Broa) reservoir to the passage of cold fronts as reflected by physical, chemical, and biological variables. **Brazilian Journal of Biology**, v. 64, n. 1, p. 177–186, 2004.

VILLAR, R.E.; MARTINEZ, J.M.; LE TEXIER, M.; GUYOT, J.L.; FRAIZY, P.; MENESES, P.R.; DE OLIVEIRA, E. A study of sediment transport in the Madeira River, Brazil, using MODIS remote-sensing images. **Journal of South American Earth Sciences**, v. 44, p. 45–54, 2013.

WALKER, H. Cyanotoxins in drinking water: fundamental concepts and solutions. CRC Press, 2025.

XIE, F.; TAO, Z.; ZHOU, X.; LV, T.; WANG, J.; LI, R. A prediction model of water in situ data change under the influence of environmental variables in remote sensing validation. **Remote Sensing**, v. 13, n. 1, 70, 2020. http://dx.doi.org/10.3390/rs13010070

YANG, H.; KONG, J.; HU, H.; DU, Y.; GAO, M.; CHEN, F. A review of remote sensing for water quality retrieval: progress and challenges. Remote Sensing, v. 14, n. 8, 1770, 2022.

ZHAO, X.; LI, Y.; CHEN, Y.; QIAO, X.; QIAN, W. Water chlorophyll-a estimation using UAV-based multispectral data and machine learning. **Drones**, v. 7, n. 2, 2022.

Submetido em 16 de junho de 2025
Aceito para publicação em 20 de agosto de 2025